Electronic Journal of Biotechnology 81 (2026) 100710

Contents lists available at ScienceDirect

Electronic Journal of Biotechnology

journal homepage: www.elsevier.com/locate/ejbt

Research article

Identification and verification of diagnostic biomarkers related to matrisome in patients with knee osteoarthritis based on machine learning algorithms ☆

Jianqiao Sun, Gongchang Yu, Yingjie Zhao, Jun Zhang, Bin Shi *

Neck-Shoulder and Lumbocrural Pain Hospital of Shandong First Medical University, Shandong First Medical University & Shandong Academy of Medical Sciences, Jinan City, Shandong Province, China

GRAPHICAL ABSTRACT

Identification and verification of diagnostic biomarkers related to matrisome in patients with knee osteoarthritis based on machine learning algorithms.

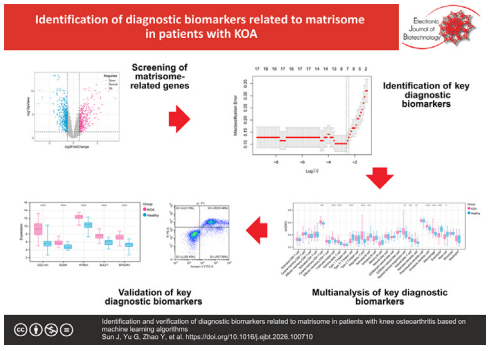

ARTICLE INFO

Article history:
Received 30 May 2025
Accepted 23 January 2026
Available online 18 March 2026

Keywords:
Biomarkers
Collagen Type I
Disease
Drug repurposing
Extracellular matrix
Gene expression profiling
Knee
Matrisome

ABSTRACT

Background: It is reported that matrisome exerts a significant function in the pathogenesis of knee osteoarthritis (KOA). Thus, this study was conducted to screen the matrisome-associated diagnostic genes for KOA.

Results: A total of 158 matrisome-related genes in KOA were obtained, then 5 diagnostic genes were screened, namely collagen type 1 alpha 1 (COL1A1), high temperature requirement factor A1 (HTRA1), SPARC (osteonectin), cwcv and kazal-like domains proteoglycan 1 (SPOCK1), sulfatase 1 (SULF1) and extracellular matrix protein 1 (ECM1). These 5 diagnostic genes were both obviously overexpressed in KOA groups relative to those in the healthy group, and both strongly associated with most immune cells, such as macrophage, eosinophil, and activated B cell. The targeted drugs for the 5 diagnostic genes contained 9-Octadecenamide, Diacerein, and Rifaximin. The mRNA and protein expression levels of the 5 diagnostic genes were consistent with the bioinformatics analysis results. Also, the viability of monosodium iodoacetate (MIA)-treated SW1353 cells was significantly decreased after upregulation of ECM1, while apoptosis showed the opposite trend. Moreover, MIA remarkably increased the phosphorylation

☆ Audio abstract available in Supplementary material.

Peer review under responsibility of Pontificia Universidad Católica de Valparaíso.

* Corresponding author.
E-mail address: bshi@sdfmu.edu.cn (B. Shi).

https://doi.org/10.1016/j.ejbt.2026.100710

Osteoarthritis
PI3K-Akt signaling pathway
Signal transduction

levels of PI3K and Akt in SW1353 cells.
Conclusions: Five matrisome-associated diagnostic genes were identified with better diagnostic values, including COL1A1, HTRA1, SPOCK1, SULF1 and ECM1. ECM1 exacerbates the progression of KOA, and PI3K-Akt signaling pathway is involved in the progression of KOA. The drugs, containing 9-Octadecenamide, Diacerein, and Rifaximin, etc., might be used for KOA treatment by targeting COL1A1, HTRA1, SPOCK1, SULF1 and ECM1.

How to cite: Sun J, Yu G, Zhao Y, et al. Identification and verification of diagnostic biomarkers related to matrisome in patients with knee osteoarthritis based on machine learning algorithms. Electron J Biotechnol 2026;81. https://doi.org/10.1016/j.ejbt.2026.100710.

1. Introduction

Knee osteoarthritis (KOA) is a familiar degenerative joint disease in clinical practice, which mainly occurs in middle-aged and elderly populations and is a common disabling disease [1,2]. KOA is mainly characterized by pain, swelling, and limited joint movement [3,4]. With the aging of the global population and the increase in obesity, as well as more and more joint injuries, the incidence rate of OA is rising [5]. According to epidemiological statistics, the incidence of KOA is relatively high at present, and the incidence of KOA in China is about 21.51% [6]. However, the pathological mechanism of OA is currently not fully clarified. Currently, KOA is usually diagnosed through symptoms and imaging examinations, and treated with physical therapy and medication [7,8]. For patients in the advanced stage of KOA, replacement surgery is required [9]. Thus, effective decision-making for diagnosis is crucial, necessitating diagnostic biomarkers for monitoring and targeted therapy to improve outcomes.

The extracellular matrix (ECM) is composed of multiple components that interact bidirectionally with surrounding cells, creating a dynamic and responsive microenvironment that mediates the homeostasis of cells and tissues [10,11]. KOA is currently indicated to be characterized by destruction of articular cartilage, and the destruction can be described as an imbalance between synthesis and degradation of ECM components [12]. ECM proteins, collectively known as matrisome, comprise collagens, proteoglycans and glycoproteins [13]. Alterations in the matrisome have been reported to be involved in numerous diseases, containing Parkinson's disease, cancer, adolescent idiopathic scoliosis, etc. [14,15,16]. For instance, Sung and Cheong [17] found that matrisome in stem-like phenotypes of gastric cancer is related to metabolic reprogramming. Notably, it was found that collagen type 1 alpha 1 (COL1A1) and COL1A2 were expressed at a low level in normal chondrocytes but highly expressed in OA, and dysregulated expression of type I collagen acts as a critical pathogenic role in OA [18,19]. In addition, the expression of matrix metalloproteinase 2 (MMP2)/MMP13 was enhanced in OA cartilage tissue, which accelerated the process of KOA cartilage degeneration by cleaving internal peptide bonds and degrading ECM components [20]. Moreover, Chen et al. [21] uncovered that Tongbi Huoluo Decoction inhibited the degradation of cartilage ECM by regulating the expression of type I collagens and MMPs to ameliorate cartilage degeneration in KOA. Currently, studies have shown that Toll-Like Receptor 4 (TLR-4), TLR-5, Interferon Regulatory Factor (IRF4), and fibulin-3 are diagnostic markers in patients with KOA [22,23]. However, given the significant role of the matrisome in KOA, finding matrisome-related biomarkers may provide insights for the diagnosis and therapy of KOA.

Herein, matrisome-associated diagnostic genes were screened by weighted gene co expression network analysis (WGCNA) and machine learning, followed by validation in *in vitro* experiments. Notably, the diagnostic value of the obtained diagnostic genes was explored, and the potential drugs in KOA were identified. This study will provide promising novel biomarkers for the diagnosis and therapy of KOA.

2. Materials and methods

2.1. Source of data

Three KOA-related datasets (GSE114007, GSE57218, and GSE51588) were acquired from Gene Expression Omnibus (GEO) database with the following inclusion criteria: (a) independent expression profile of KOA, (b) dataset containing grouping information for KOA and healthy controls, (c) the total number of samples in the dataset should be at least 30, and (d) test specimens in the dataset extracted from human *Homo sapiens* knee cartilage tissue. GSE114007 contained 20 KOA and 18 healthy control samples, GSE57218 included 23 KOA and 7 healthy control samples, and GSE51588 served as a validation dataset and comprised 40 KOA and 10 healthy control samples. The "sva" package [24] (version 3.50.0) was employed to eliminate batch effects on GSE114007 and GSE57218, which were combined as a training dataset. The flow chart of this study is illustrated in Fig. 1.

2.2. Screening of DEGs and GSEA analysis

Differentially expressed genes (DEGs) between the KOA and healthy group were pinpointed employing "limma" [25] (version 3.58.1) with criteria set at |log2 fold change (FC)| $\geq$ 0.5 and *p*. adj < 0.05 [26]. The *p*-value was corrected using the Benjamini-Hochberg (BH) method. Besides, Gene Set Enrichment Analysis (GSEA) analysis was carried out to identify differentially Kyoto Encyclopedia of Genes and Genomes (KEGG) pathways between KOA and the healthy group with the threshold of |normalized enrichment score (NES)| > 1 and *p*. adj < 0.05 [27].

2.3. Acquisition of matrisome-related genes in KOA

The "WGCNA" [28] (version 1.72-5) was utilized to screen module genes associated with KOA with MAD (absolute median deviation) Top 5000 gene expression data as input matrix, and KOA and healthy as phenotype traits. Firstly, the "power" value [29] was employed to analyze the square of the association coefficient between average connectivity, connectivity (k), and p(k) with the "pickSoftThreshold" function. Using clustering and dynamic pruning techniques, parameters such as minModuleSize = 100 [30] were utilized to group genes with high correlations into modules. Then, modules closely associated with phenotype traits were chosen. Subsequently, after 1062 matrisome-related genes were searched by evaluating the pertinent literature [31] (Table S1), the common genes between DEGs, module genes, and matrisome-related genes were ascertained. Then, the enriched analysis was applied on these matrisome-associated genes in

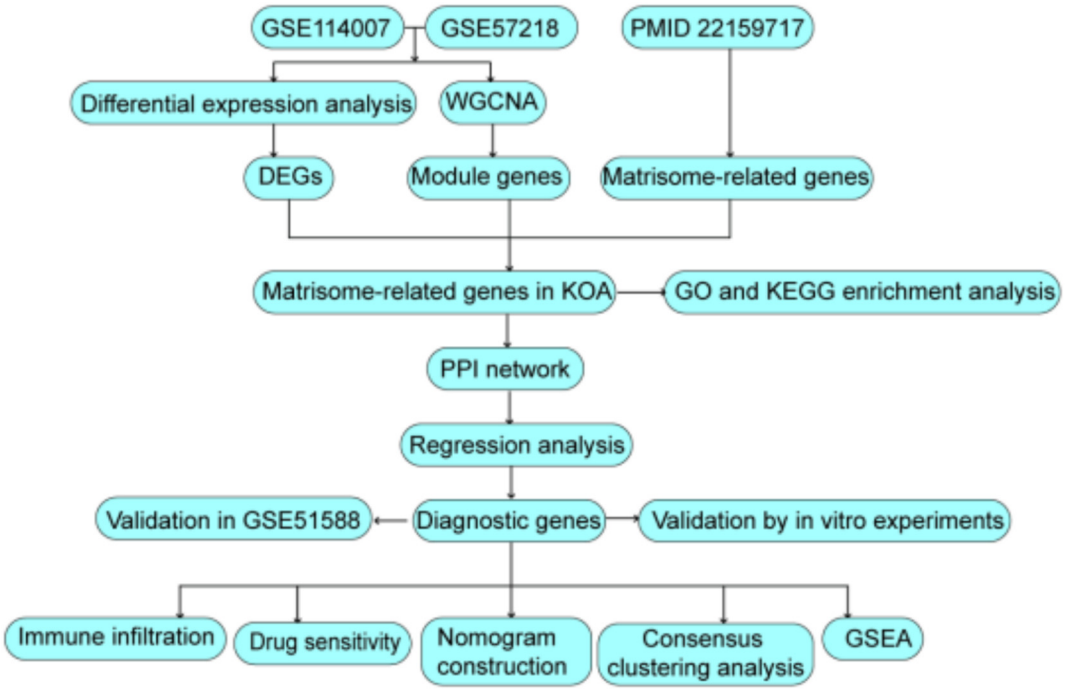

Fig. 1. Flow chart of this study.

KOA by using the "clusterProfiler" package [32] (version 4.10.1) with the threshold of *p*. adj < 0.05.

2.4. Protein-Protein Interaction (PPI) network establishment

The protein interaction relationships of the matrisome-related genes in KOA were predicted by "STRING" database [33] (version 11.0), and the PPI network was built with the cutoff value of combined score = 0.4 [34]. Besides, four topology analysis algorithms of "cytoHubba" plug-in in "Cytoscape" [35] (version 3.8.2), Maximal Clique Centrality (MCC), Edge Percolated Component (EPC), Maximum Neighborhood Component (MNC), and Degree, were utilized to explore hub genes in PPI networks.

2.5. Identification of diagnostic genes

The feature genes of KOA were acquired using Least Absolute Shrinkage and Selection Operator (LASSO) [36], random forest (RF) [37] and Support Vector Machine Recursive Feature Elimination (SVM-RFE) [38]. LASSO regression was performed with 10-fold cross-validation and the parameter of "standardize = TRUE"; RF was conducted with the parameters of "nodesize = 5, ntree = 500–1000", and the optimal value was selected through cross-validation and tuneRF; SVM-RFE was carried out with the parameter of "cv folds = 10, kernel = linear", and the optimal value was selected through cross-validation (grid search). The "glmnet" [39] (version 4.1-8), "randomForest" [40] (version 4.7-1.1) and "e1071" [41] (version 1.7-14) were employed to conduct LASSO, RF and SVM-RFE analyses, separately. In addition, the common genes obtained from three machine learning algorithms were acquired as the diagnostic genes of KOA. Besides, the diagnostic gene expression levels were assessed in training and validation datasets, and "pROC" [42] (version 1.18.5) was utilized to draw the ROC curve to explore the diagnostic ability of diagnostic genes with the classification information and gene expression levels, and the AUC values were calculated using "Python". In addition, the "GeneMANIA" database was employed to conduct a PPI network on the diagnostic genes with the parameters of "Max resultant genes = 20, Max resultant attributes = 20, automatically selected weighting", as well as GSEA analysis.

2.6. Nomogram construction and potential drugs prediction

A nomogram consists of a set of scales that each scale represents a characteristic of the study population. If there are interaction terms in the original regression model, there will be several scales representing certain combinations of interacting variables. Nomogram is actually a visualization of a complex model equation in which the behavior of a predictor is represented in scales [43]. In clinical medicine, the tool is widely used for the prediction of patients' outcomes, considering the clinical characteristics of patients. Based on the magnitudes of the regression coefficients of all independent variables, a scoring standard was established. A score to each value level of each independent variable was assigned, and a total score can be calculated for each sample. Then, the probability of the occurrence of each sample can be calculated through the conversion function between the score and the probability of the outcome occurrence. The "rms" package [44] (version 6.8-0) was utilized to construct a nomogram. Decision curve analysis (DCA) is a valuable tool in clinical research for evaluating models. The calibration and DCA curves were drawn to assess the predictive ability of the nomogram by using "rmda" package [45]. In addition, the underlying drugs were searched in "DSigDB" database [46], and the correlation between potential drugs and diagnostic genes was investigated.

2.7. Association between immune cells and diagnostic genes

"ssGSEA" algorithm [47] was employed to assess the proportion of 28 immune cells with the parameters of "tau = 0.25, min.sz = 5, abs.ranking = FALSE", and differences in the proportion of immune cells in KOA and healthy groups were compared using the Wilcoxon test. Then, the "Spearman" function in "ggplot2" package (version 3.5.0) was employed to analyze the correlations between immune cells and immune cells or immune cells and diagnostic genes.

2.8. Consensus clustering analysis

"ConsensusClusterPlus" package (v 1.66.0) [48] was utilized to perform consensus clustering analysis on the diagnostic genes by the k-means method [49], and the KOA samples were divided into different subtypes. Then, the difference in fraction of immune cell in clusters was compared.

2.9. Sample collection

The blood samples were collected from 6 KOA patients and 6 healthy controls. The inclusion criteria were as follows: (a) patients aged 40–75 years; (b) Those presenting with knee pain for at least 3 months; (c) those with OA in at least one knee according to the American College of Rheumatology Classification Criteria; (d) those reporting a minimum average overall knee pain intensity of 40 on a 100-mm visual analog score (VAS) for most days in the last month [50]. The exclusion criteria were as follows: (a) patients with knee joint injection within the last 6 months; (b) those who have taken oral corticosteroids within the last month; (c) patients with systemic arthritic conditions; (d) those who have participated in hip or knee muscle strengthening programs within the last 3 months. Healthy controls were those with no symptoms of knee disease and knee pain. Baseline characteristics of the total participants are illustrated in Table S2.

2.10. Cell culture

The human chondrosarcoma cell line (SW1353) has been widely used for the investigation of KOA. In cultures, chondrocyte treated with monosodium iodoacetate (MIA), an inhibitor of glyceraldehyde-3-phosphate dehydrogenase that can cause chondrocyte death, is the generally accepted cell model to stimulate the progression of KOA in humans. Human chondrosarcoma cell line SW1353 was purchased from the American Type Culture Collection (Rockville, MD) and cultivated in Dulbecco's Modified Eagle Medium (DMEM) medium supplemented with 10% fetal bovine serum (FBS) under normal conditions. When the cells reached 80–90% confluence, the cells were subcultured. Attached cells were treated with 5 μM MIA (Sigma-Aldrich, St Louis, MO) for 24 h to simulate the KOA model *in vitro* according to a previous study [51]. For transfection, the SW1353 cells were grown to 70–80% confluence and transfected with lentivirus composing either over-expression (oe)-ECM1 or oe-Negative Control (NC) for 24 h. Cell Counting Kit-8 (CCK-8) [52] was employed to measure the cell viability based on the CCK-8 kit (#40203ES60, Yeasen).

2.11. Flow cytometry

Apoptosis of SW1353 cells was measured using Annexin V-Fluorescein Isothiocyanate (FITC) apoptosis detection kit (#C1062S, Beyotime) based on the manufacturer's instructions [53]. Briefly, 5–10 × 10^4 suspended cells were centrifuged for 5 min; then, 195 μL Annexin V-FITC binding solution was added. Subsequently, 5 μL of Annexin V-FITC was added, followed by 10 μl of propidium iodide staining solution. Cells were examined using flow cytometer (Beckman, CytoFLEX S).

2.12. Enzyme-linked immunosorbent assay (ELISA)

The levels of Collagen II (#ab285250, abcam) were assessed by an ELISA commercial kit according to the manufacturer's instructions [54] and repeated three times. Distilled water was used to dilute the 20-fold concentrated washing solution to the original concentration. Fifty μL standard sample was added to the standard sample well, and then, 40 μL sample diluent was added. Absorbance at 450 nm was measured by a microplate reader.

2.13. Quantitative reverse transcriptase polymerase chain reaction (qRT-PCR)

Total RNA extraction was performed using TRIzol reagent in blood samples and SW1353 cells and reverse-transcribed into cDNA by FastKing-RT SuperMix (#KR118-02, TIANGEN). The qRT-PCR [55] was carried out with SYBR Green PCR Master mix (#A4004M, Lifeint) and 1 μg total RNA. Primers for the target genes were designed by Primer Premier 5.0, with lengths of 18–27 bp, GC content (the ratio of guanine to cytosine bases) between 40% and 60%. The utilized primers are shown in Table 1. Expression levels of diagnostic biomarkers were assessed utilizing the $2-\Delta\Delta CT$ method, and GAPDH served as an internal control.

2.14. Western blot analysis

Total protein in blood samples of 6 KOA patients and 6 healthy controls was collected utilizing RIPA lysis buffer (#P0013B, Beyotime), and a Bicinchoninic Acid (BCA) protein quantification kit (#P0012, Beyotime) was utilized to evaluate protein concentrations. Proteins (20 μg/well) analyzed using Sodium Dodecyl Sulfate PolyAcrylamide Gel Electrophoresis (SDS-PAGE) were transferred onto polyvinylidenefluoride (PVDF) membranes (#FFP24, Beyotime). Membranes were blotted with antibodies of anti-COL1A1 (1:1000; #ab138492, abcam), anti-HTRA1 (1:1000; #ab274322, abcam), anti-SPOCK1 (1:1000; #ab229935, abcam), anti-SULF1 (1:1000; #ab32763, abcam), anti-ECM1 (1:10000; #ab253185, abcam), anti-PI3K (1:1000; #ab32089, abcam), anti-p-PI3K (1:1000; #4228 T, Cell Signaling Technology), anti-Akt (1:1000; #abs131788, Absin Bioscience Inc.), anti-p-Akt (1:1000; #4058 L, Cell Signaling Technology), and anti-GAPDH (1:10000; #ab181602, abcam). For secondary antibody, Peroxidase-Conjugated Goat anti-rabbit IgG (H&L) (1:10000; #A0208, Beyotime) was judiciously employed. The membranes were evaluated using an electrochemical luminescence (ECL) reagent (#P1000, APPLYGEN). Quantification was performed using ImageJ software.

2.15. Statistical analysis

Statistical analysis was fulfilled by GraphPad 7.0 software. Experimental data were presented as mean ± standard deviation (SD). One-way ANOVA was used, followed by Tukey's post-hoc test for comparisons to accurately evaluate the differences between

Table 1
Primers used in RT-PCR.

Gene	Sequence (5′-3′)
COL1A1 (Forward)	CGATGGATTCCAGTTCGAGT
COL1A1 (Reverse)	TTTTGAGGGGGGTTCAGTTTG
HTRA1 (Forward)	CAAAGCCAAAGAGCTGAAGG
HTRA1 (Reverse)	ACCATGTTCAGGGTGCTTTC
SPOCK1 (Forward)	CAGCCTGTCCACACAAAAGC
SPOCK1 (Reverse)	CCATCGATTTGGGGGTTCCA
SULF1 (Forward)	TGCTCAAAGTGACGGGTTCTTGGT
SULF1 (Reverse)	GTTGGTCGGTTCAAATGCAGGGTT
ECM1 (Forward)	TGCTGTGACCTGCCATTTCC
ECM1 (Reverse)	AAGCAGTTGACCTGTTCATCCC
MMP-13 (Forward)	CACCCTCAGCAGGTTGAGCC
MMP-13 (Reverse)	ACCGCAGCACTGAGCCTTTT
ADAMTS4 (Forward)	GAGGGAGGCACCCCTAACT
ADAMTS4 (Reverse)	CCTTGACGTTGCACATGGGA
GAPDH (Forward)	ATGGGGAAGGTGAAGGTCG
GAPDH (Reverse)	TGGAAGATGGTGATGGGATTT

qRT-PCR: quantitative reverse transcriptase polymerase chain reaction.

groups. When |log2FC| > 0.5 and $p < 0.05$ in experiments, the difference was significant.

3. Results

3.1. Identification of DEGs in KOA

In the detection and removal of batch effects, the Uniform Manifold Approximation and Projection (UMAP) curve can assist researchers in observing the distribution differences between different batches, thereby evaluating the impact of batch effects. Herein, the UMAP curves showed the samples in GSE114007 and GSE57218 datasets after eliminating batch effects (Fig. 2A). A total of 865 DEGs were acquired, composing 388 upregulated and 477 downregulated DEGs (Fig. 2B–C). Also, GSEA analysis revealed that numerous pathways related to extracellular matrix, immunity, and metabolism were involved in the molecular mechanism of KOA (Fig. 2D–E).

3.2. Screening of matrisome-related genes in KOA

In order to maximize the fulfillment of the scale-free network distribution premise, the value of "power" was chosen as when the correlation coefficient reached 0.85, which is "power" = 8 (Fig. 3A). Then, total 7 modules were integrated with parameter of minModuleSize = 100 (Fig. 3B). Furthermore, the red module uncovered the strongest significant association with KOA (r = 0.61, p = 7e-09), and the red module contained 363 genes, which were considered as the module genes (Fig. 3C). Then, 58 matrisome-related genes in KOA were screened by intersecting 865 DEGs, 363 module genes, and 1062 matrisome-related genes (Fig. 3D; Table S3). Then, the enrichment analysis of 58 matrisome-related genes in KOA was conducted (Fig. 3E). Besides, the PPI network of 58 matrisome-related genes in KOA was constructed, including 56 nodes and 438 edges (Fig. 3F; Table S4).

3.3. Diagnostic biomarkers identification

LASSO, RF and SVM-RFE algorithms were applied to search feature genes, and total 7, 56, and 7 feature genes were identified, respectively (Fig. 4A–C). Moreover, 5 overlapped genes obtained as the diagnostic genes (Fig. 4D), namely COL1A1, high temperature requirement factor A1 (HTRA1), SPARC (osteonectin), cwcv and kazal-like domains proteoglycan 1 (SPOCK1), sulfatase 1 (SULF1) and extracellular matrix protein 1 (ECM1). Furthermore, the ROC curve shown that the Area Under Curves (AUCs) of diagnostic genes were all above 0.85 in training dataset, as well as above 0.78 in the verification dataset (Fig. 4E,F). Moreover, the expression levels of the 5 diagnostic genes were analyzed in training and validation datasets, and these 5 diagnostic genes were both obviously overexpressed in KOA groups relative to those in the healthy group (both $p < 0.01$; Fig. 4G,H).

3.4. Nomogram construction and association between immune cell and diagnostic genes

A nomogram of these 5 diagnostic genes was established (Fig. 5A), and the predictive performance of the nomogram was assessed using a calibration curve (Fig. 5B), implying that the nomogram possessed high precision for predicting KOA. In addition, the DCA curve indicated that the gray line curve was lower than the nomogram curve, indicating that the nomogram possessed better clinical benefits for the patient (Fig. 5C). Moreover, to more intuitively explore the clinical effectiveness of the nomogram, a clinical impact curve was drawn based on the DCA curve. The "Number high risk with event" curve was very close to the "Number high risk" curve when the high-risk threshold ranges from 0.7 to 1, indicating that the nomogram had good predictive ability (Fig. 5D). Besides, "ssGSEA" algorithm uncovered that the fraction of 13 immune cells presented significant differences between KOA and healthy samples (Fig. 5E), including macrophage, eosinophil, and mast cell. Then the association between immune cells and immune cells or diagnostic genes and immune cells was investigated (Fig. 5F,G), and the results found that these 5 diagnostic genes (COL1A1, HTRA1, SPOCK1, SULF1 and ECM1) were both strongly associated with most immune cells.

3.5. PPI network, potential drugs prediction and GSEA analysis

Based on "GeneMANIA" database, the PPI network of the 5 diagnostic genes (COL1A1, HTRA1, SPOCK1, SULF1 and ECM1) was established (Fig. 6A), and these 5 diagnostic genes interacted with 20 genes. Besides, drugs that interacted with the 5 diagnostic genes were obtained through the "DSigDB" database (Fig. 6B), containing 9-Octadecenamide, Diacerein, and Rifaximin, etc., which might be used to treat KOA via targeting these 5 genes. Also, GESA analysis revealed the KEGG pathways in which these diagnostic genes are involved (Fig. 6C).

3.6. Identifying KOA-associated molecular subtypes

By improving the clustering variable (k) from 2 to 9, the results shown that when k = 2, the intragroup associations were the highest, suggesting that the KOA samples could be well separated into two clusters according to the obtained 5 diagnostic genes, namely C1 (27 KOA samples) and C2 (26 KOA samples) (Fig. 7A). PCA analysis observed a consistent division of samples into the two subtypes with stability (Fig. 7B). Also, the 5 diagnostic genes expression levels were assessed in subtypes, and these 5 diagnostic genes were both obviously overexpressed in C1 relative to those in C2 (both $p < 0.05$; Fig. 7C). Besides, the fraction of 12 immune cells presented significant differences between C1 and C2 (both $p < 0.05$; Fig. 7D), including effector memory CD8 T cell, activated CD4 T cell, central memory CD4 T cell, T follicular helper cell, gamma delta T cell, type 1 T helper cell, type 17 T helper cell, regulatory T cell, CD56dim natural killer cell, myeloid derived suppressor cell, activated dendritic cell, and macrophage.

3.7. ECM1 and PI3K-Akt signaling pathway involved in the progression of KOA

To confirm the expression of 5 diagnostic genes in KOA, the qRT-PCR and western blot were conducted. The mRNA and protein expression levels of these 5 diagnostic genes were both obviously upregulated in KOA groups relative to those in the healthy group, as well as the mRNA expression of cartilage degeneration-related genes: MMP-13 and ADAM metallopeptidase with thrombospondin type 1 motif 4 (ADAMTS4) (both $p < 0.05$; Fig. 8A,B). Considering the higher degree of ECM1 in PPI (Fig. 3F and Table S4), few studies have reported the role of ECM1 in KOA, and thus, ECM1 was chosen to further explore in KOA. To explore the function of ECM1 in KOA, the transfection efficiency was measured after MIA-treated SW1353 cells transfecting with oe-ECM1 (Fig. 8C). Then the results uncovered that the viability of MIA-treated SW1353 cells was obviously decreased after upregulation of ECM1, while apoptosis showed the opposite trend (both $p < 0.01$; Fig. 8D,E). Moreover, the content of Collagen II in MIA-treated SW1353 cells was obviously suppressed after upregulation of ECM1 compared to that in the control group ($p < 0.05$; Fig. 8F). Besides, to verify whether

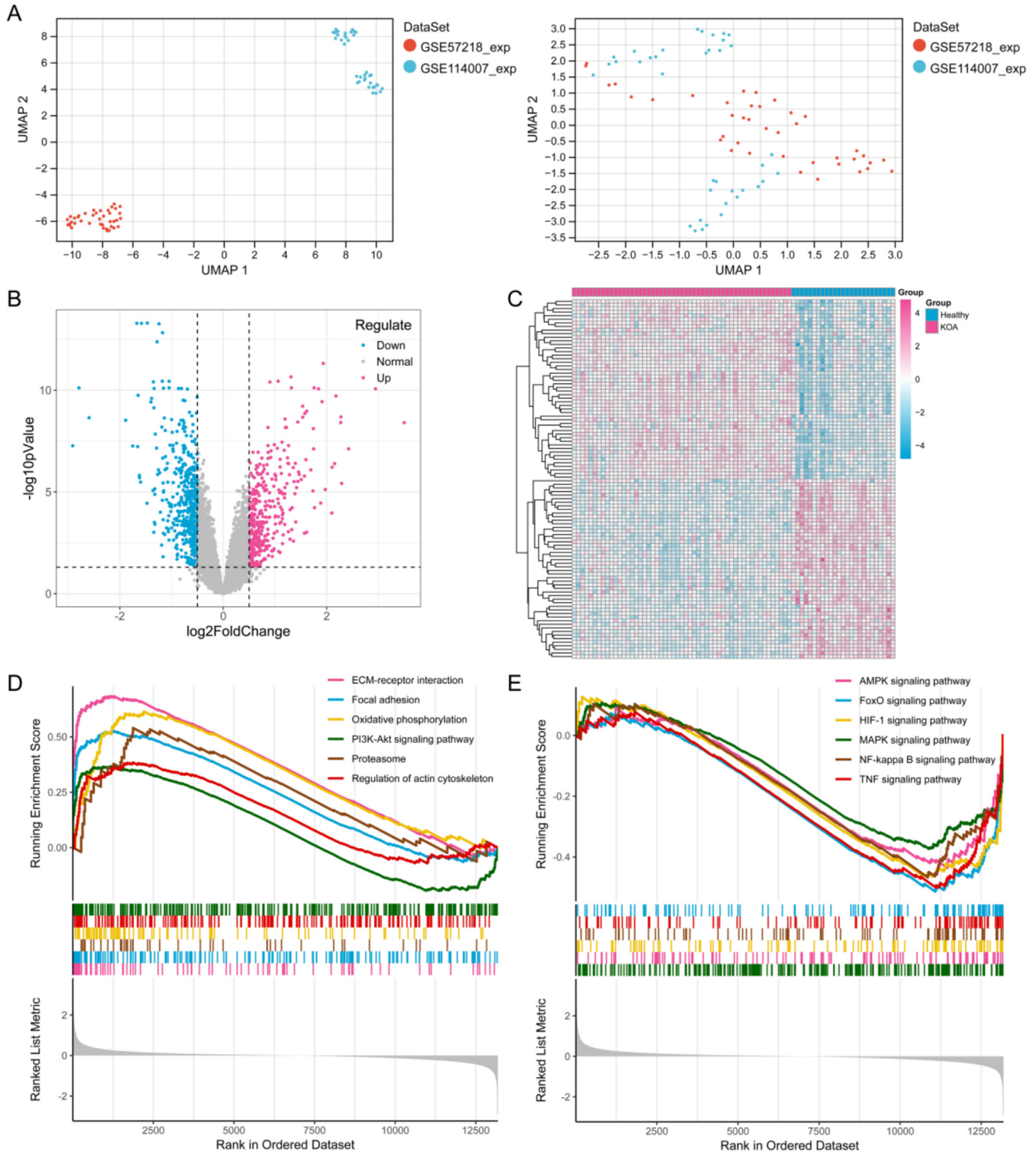

Fig. 2. Identification of DEGs in KOA. (A) The samples in GSE114007 and GSE57218 datasets before (left) and after (right) eliminating batch effects. (B) Volcano map of DEGs. Red and blue represent upregulated genes and downregulated genes, respectively, whereas gray indicates no significant difference. (C) Heatmap of Top 50 DEGs. Columns correspond to the samples, and rows correspond to the genes. Upregulated (D) and downregulated (E) pathways identified by GSEA analysis. DEGs: differentially expressed genes; KOA: knee osteoarthritis; GSEA: Gene Set Enrichment Analysis. (For interpretation of the references to color in this figure legend, the reader is referred to the web version of this article.)

the PI3K-Akt signaling pathway is involved in the progression of KOA, the protein expression level of PI3K/Akt pathway-related markers was detected. As shown in Fig. 8G, MIA remarkably increased the phosphorylation levels of PI3K and Akt in SW1353 cells. These findings suggested that ECM1 and PI3K-Akt signaling pathway are involved in the progression of KOA.

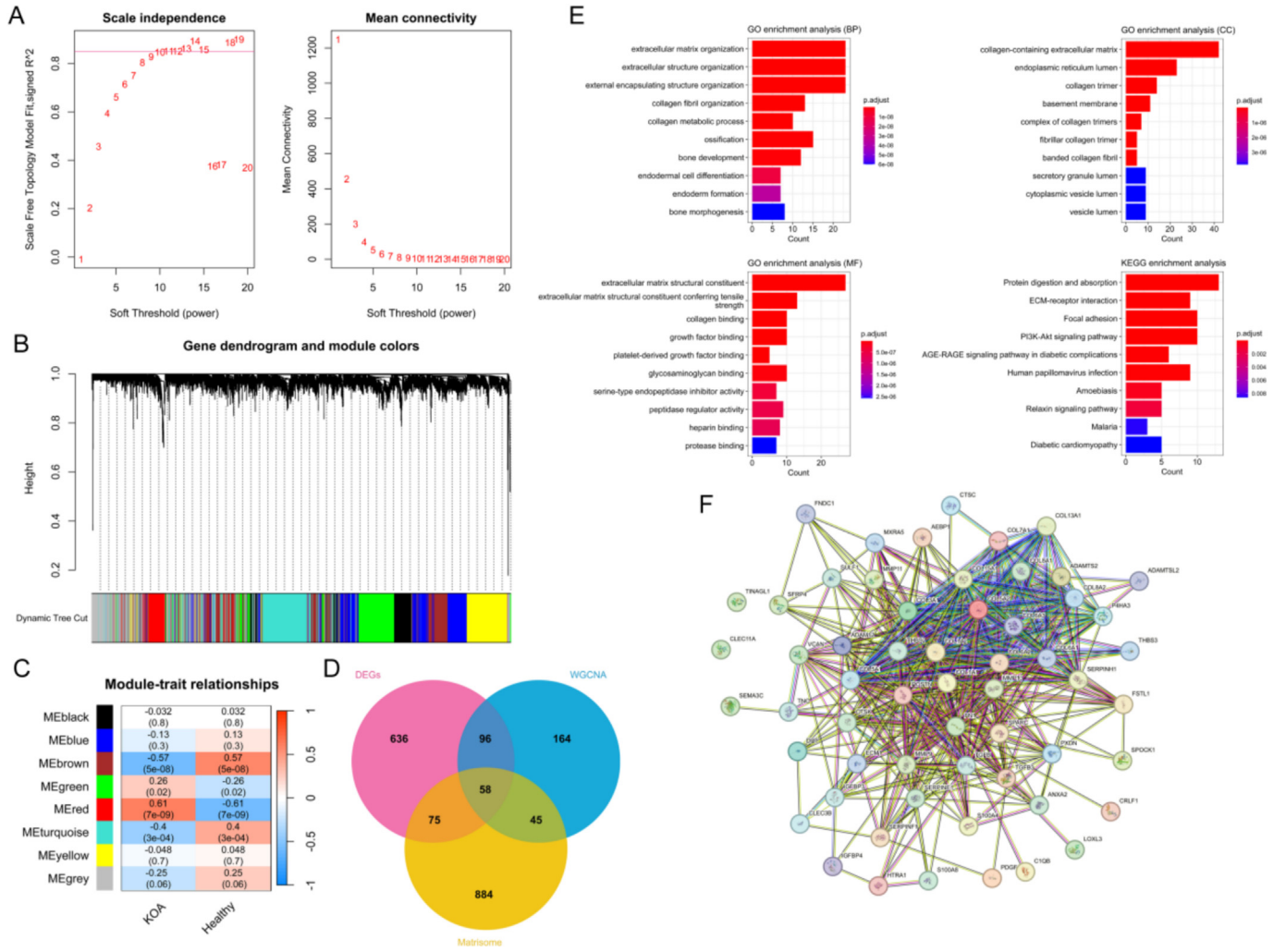

Fig. 3. Screening of matrisome-related genes in KOA. (A) Hierarchical clustering of samples and selection of the weight parameter "power" of the adjacency matrix and the mean connectivity. (B) Tree diagram for module division. Each branch represents a gene, and each color represents a module in the constructed gene co-expression network by WGCNA. The color band shows the results obtained from the automatic single-block analysis. (C) Relationships between module and trait. (D) Venn diagram of 58 matrisome-related genes in KOA. (E) Enrichment analysis of 58 matrisome-related genes in KOA. The X-axis and Y-axis show the gene count and full names of the processes, respectively, and the color and size of each column represent the P value and gene count, respectively. (F) PPI network of 58 matrisome-related genes in KOA. KOA: knee osteoarthritis; PPI: Protein-Protein Interaction.

4. Discussion

KOA is a familiar chronic progressive joint disease in middle-aged and elderly people [56]. In this study, by intersecting 865 DEGs, 363 genes in red module, and 1062 matrisome-related genes, a total of 58 matrisome-related genes in KOA were screened. To explore the molecular mechanism, the enrichment analysis of 58 matrisome-related genes in KOA was conducted. The results shown that these 58 genes are mainly enriched in protein digestion and absorption, ECM-receptor interaction, and PI3K-Akt signaling pathway. It is reported that the interaction between ECM and cellular receptors is one of the momentous pathways participated in the progression of many diseases [57,58]. In addition, Zhong et al. [59] utilized bioinformatics technology to screen the hub genes of OA, and the hub genes were primarily related to the protein digestion and absorption pathway. Numerous studies elucidated that the PI3K/AKT pathway participated in the progression of OA [60]. For instance, Xu et al. [61] found that SIRT3 ameliorates OA through the PI3K/Akt/mTOR pathway to regulate chondrocyte autophagy and apoptosis. Chen et al. [62] emphasized that icariin via the PI3K/Akt/mTOR/ULK1 signaling pathway attenuated OA. Notably, Wang et al. [63] also found that the OA-related genes were primarily enriched in ECM-receptor interaction and PI3K-Akt signaling pathways. In this study, to verify whether the PI3K-Akt signaling pathway is involved in the progression of KOA, the protein expression levels of PI3K/Akt pathway-related markers were detected. The results found that MIA remarkably increased the phosphorylation levels of PI3K and Akt in SW1353 cells. These findings suggested that the PI3K-Akt signaling pathway is involved in the progression of KOA.

Most importantly, feature genes were searched using LASSO, RF and SVM-RFE algorithms, and 5 overlapped genes were acquired as the matrisome-related diagnostic genes, namely COL1A1, HTRA1, SPOCK1, SULF1 and ECM1. COL1A1 is a member of the collagen family and participates in epithelial-mesenchymal transition [64]. Aborehab and El Bishbishy [65] have uncovered that fruit peels [*Mangifera indica* L. (mango), *Citrus sinensis* L. (orange), *Cucumis melo* L. (cantaloupe), and *Punica granatum* L. (pomegranate)] in a monosodium iodoacetate exert a significant chondroprotection function in OA through COL1A1 downregulation. HTRA1, a serine protease, regulates a series of signaling pathways that drive fundamental biological processes [66]. It is reported that HTRA1 overex-

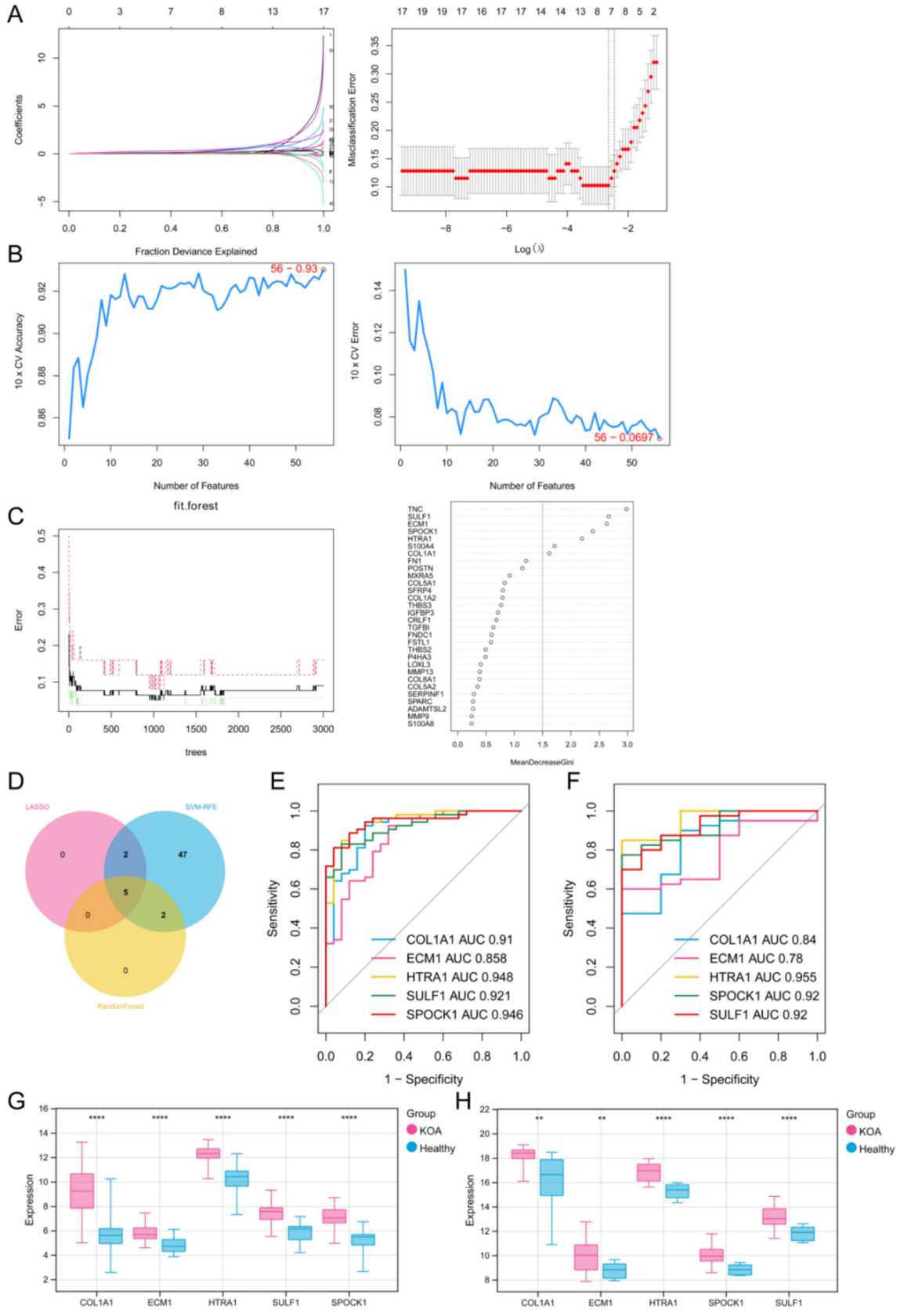

Fig. 4. Diagnostic biomarkers identification. (A) Feature genes obtained using the LASSO logistic regression model (covariates are selected using the regularization parameter λ) (A), SVM-RFE model (B), and random forest model (C). (D) Venn diagram of 5 diagnostic genes. ROC curve of 5 diagnostic genes in training (E) and verification (F) datasets. The expression level of 5 diagnostic genes in training (G) and verification (H) datasets. Red and blue represent KOA and healthy groups, respectively. $^{**}p < 0.01$, and $^{****}p < 0.0001$. LASSO: Least Absolute Shrinkage and Selection Operator; SVM-RFE: Support Vector Machine Recursive Feature Elimination; ROC: Receiver Operating Characteristic. (For interpretation of the references to color in this figure legend, the reader is referred to the web version of this article.)

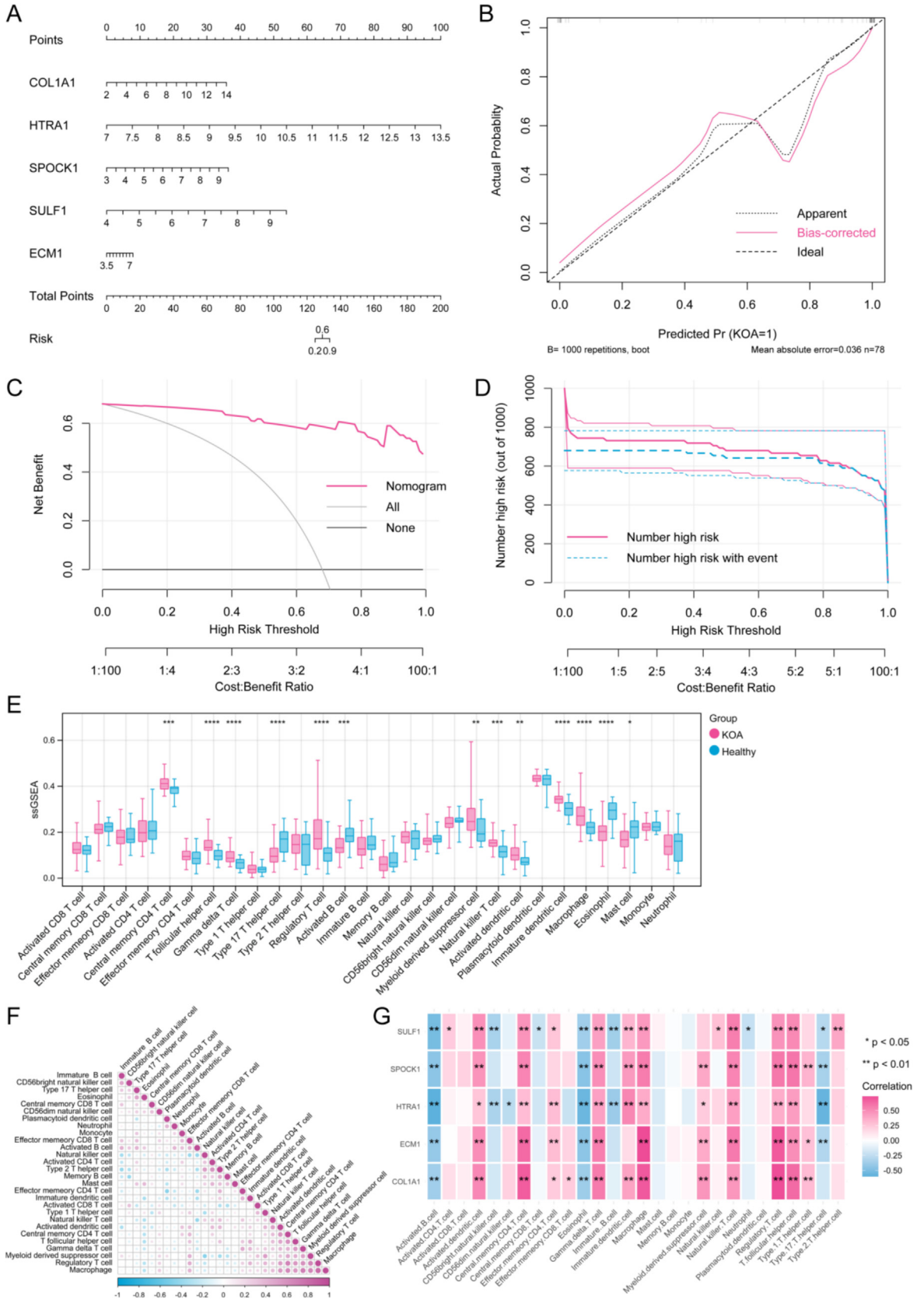

Fig. 5. Nomogram construction and association between immune cell and diagnostic genes (COL1A1, HTRA1, SPOCK1, SULF1 and ECM1). (A) Constructed nomogram. (B) Calibration curve. (C) DCA curve evaluated the clinical value of nomogram. The gray curve represents the change in the net benefit rate for all treatments with respect to the probability threshold, providing a baseline for comparison when evaluating predictive models. (D) Evaluation of the clinical impact curve of nomogram based on DCA curve. "Number high risk with event" usually refers to identifying or classifying high-risk individuals or situations according to the occurrence of specific events. (E) Difference in the fraction of 28 immune cells between KOA and healthy samples. Red and blue represent KOA and healthy groups, respectively. (F) Correlation between immune cells and immune cells. (G) Correlation between 5 diagnostic genes and immune cells. *$p < 0.05$, **$p < 0.01$, ***$p < 0.001$ and ****$p < 0.0001$. DCA: Decision curve analysis; KOA: knee osteoarthritis. (For interpretation of the references to color in this figure legend, the reader is referred to the web version of this article.)

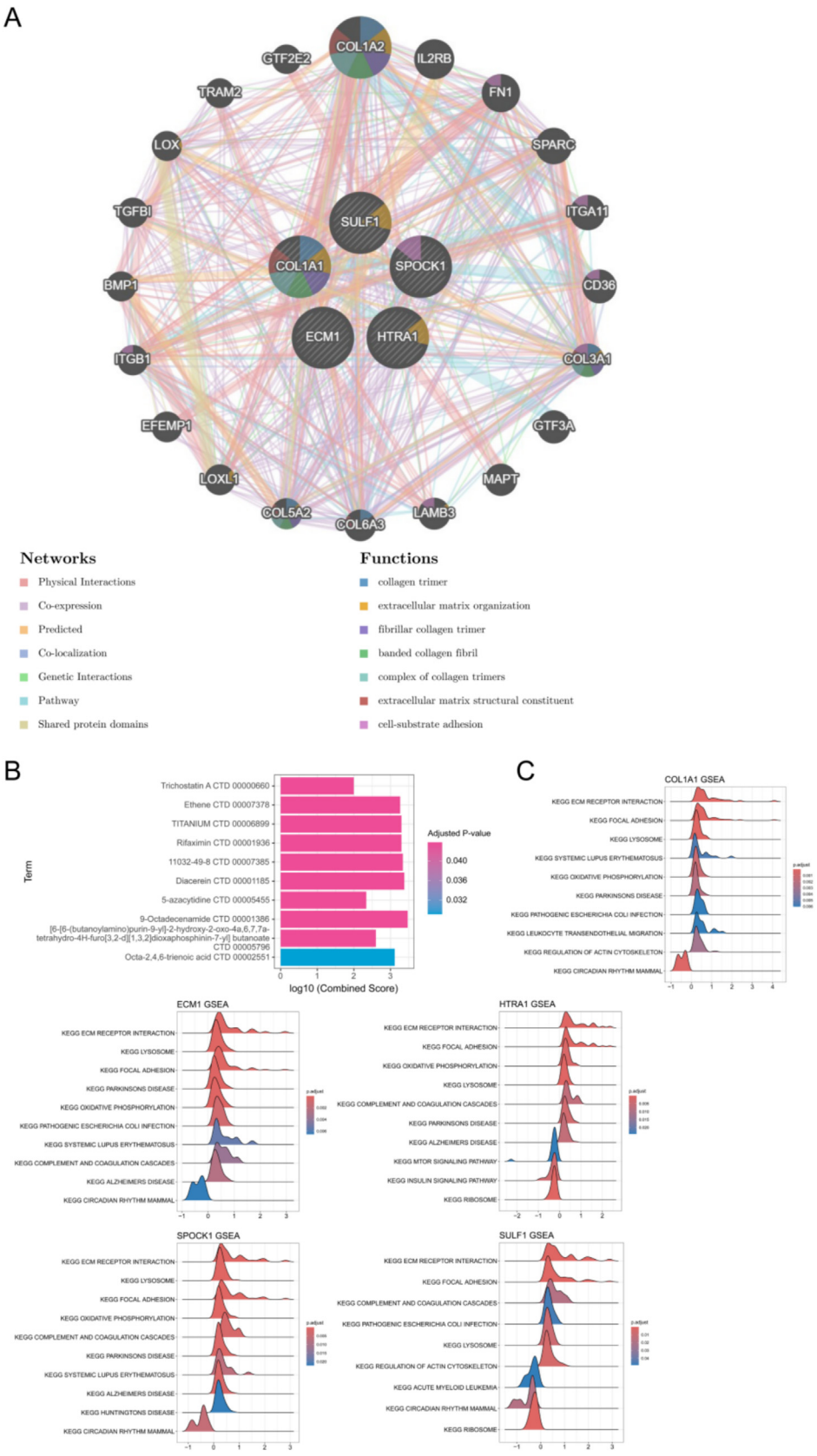

Fig. 6. PPI network, potential drugs prediction and GSEA analysis of 5 diagnostic genes. (A) PPI network. (B) Bar chart of the drugs that interacted with the 5 diagnostic genes. The color of each column represents the *p*-value. (C) KEGG pathways in which these diagnostic genes are involved. PPI: Protein-Protein Interaction; GSEA: Gene Set Enrichment Analysis; KEGG: Kyoto Encyclopedia of Genes and Genomes.

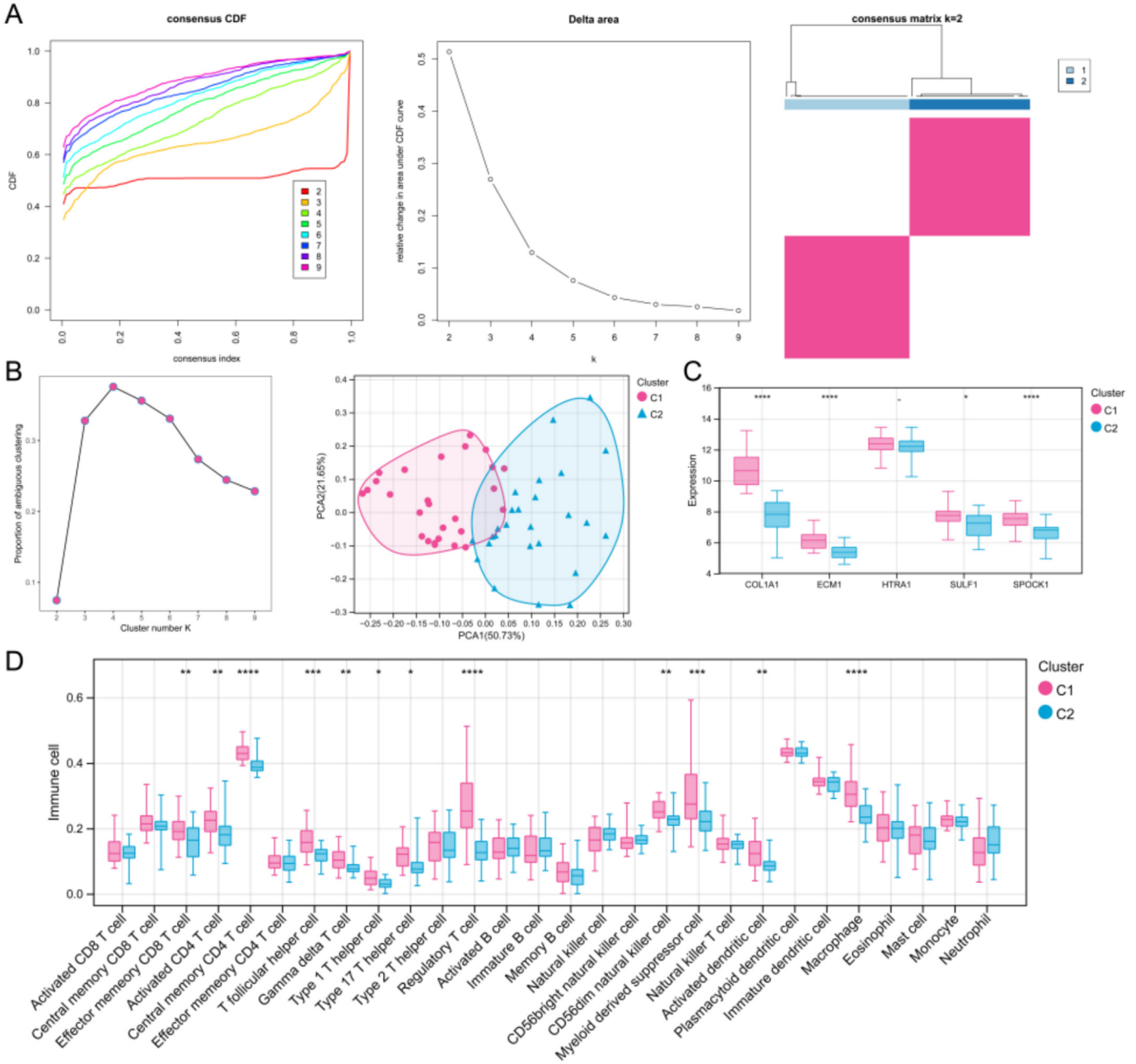

Fig. 7. Identifying KOA-associated molecular subtypes. (A) KOA patients were grouped into two clusters according to the consensus clustering matrix (k = 2). (B) PCA analysis. (C) The expression level of 5 diagnostic genes in subtypes. Red and blue represent C1 and C2 subtypes, respectively. (D) Difference in the fraction of immune cells between C1 and C2 subtypes. Red and blue represent C1 and C2 subtypes, respectively. $^{*}p < 0.05$, $^{**}p < 0.01$, $^{***}p < 0.001$ and $^{****}p < 0.0001$. KOA: knee osteoarthritis; PCA: Principal component analysis. (For interpretation of the references to color in this figure legend, the reader is referred to the web version of this article.)

pression diminishes osteoblastogenesis by upregulating Nupr1 [67]. Otsuki et al. [68] shown that the expression of SULF1 in OA cartilage was higher relative to normal human articular cartilage. Besides, Feng et al. [69] highlighted that upregulation of ECM1 in knee joints facilitates the progression of OA. Furthermore, the ROC curve shown that AUCs of diagnostic genes were all above 0.85 in the training dataset, as well as above 0.78 in the verification dataset, which suggests that these 5 diagnostic genes have good diagnostic capability performance. Notably, the mRNA and protein expression levels of the 5 diagnostic genes were consistent with the bioinformatics analysis results. Furthermore, this study also found that the viability of MIA-treated SW1353 cells was significantly decreased after upregulation of ECM1, while apoptosis showed the opposite trend. These findings fully emphasize that ECM1 exacerbates the progression of KOA.

Accumulating evidence has demonstrated that low-grade inflammation mediated by macrophage exerts a significant function in OA [70]. Zhang et al. [71] found that synovial macrophage M1 polarization, partially via R-spondin-2, exacerbated experimental OA. Blackler et al. [72] indicated that targeted activation of synovial macrophages mediated by signal transducer and activator of transcription 6 (STAT6) can improve pain in experimental KOA. Eosinophils exert important functions in defense against parasitic, fungal, viral, and bacterial infections

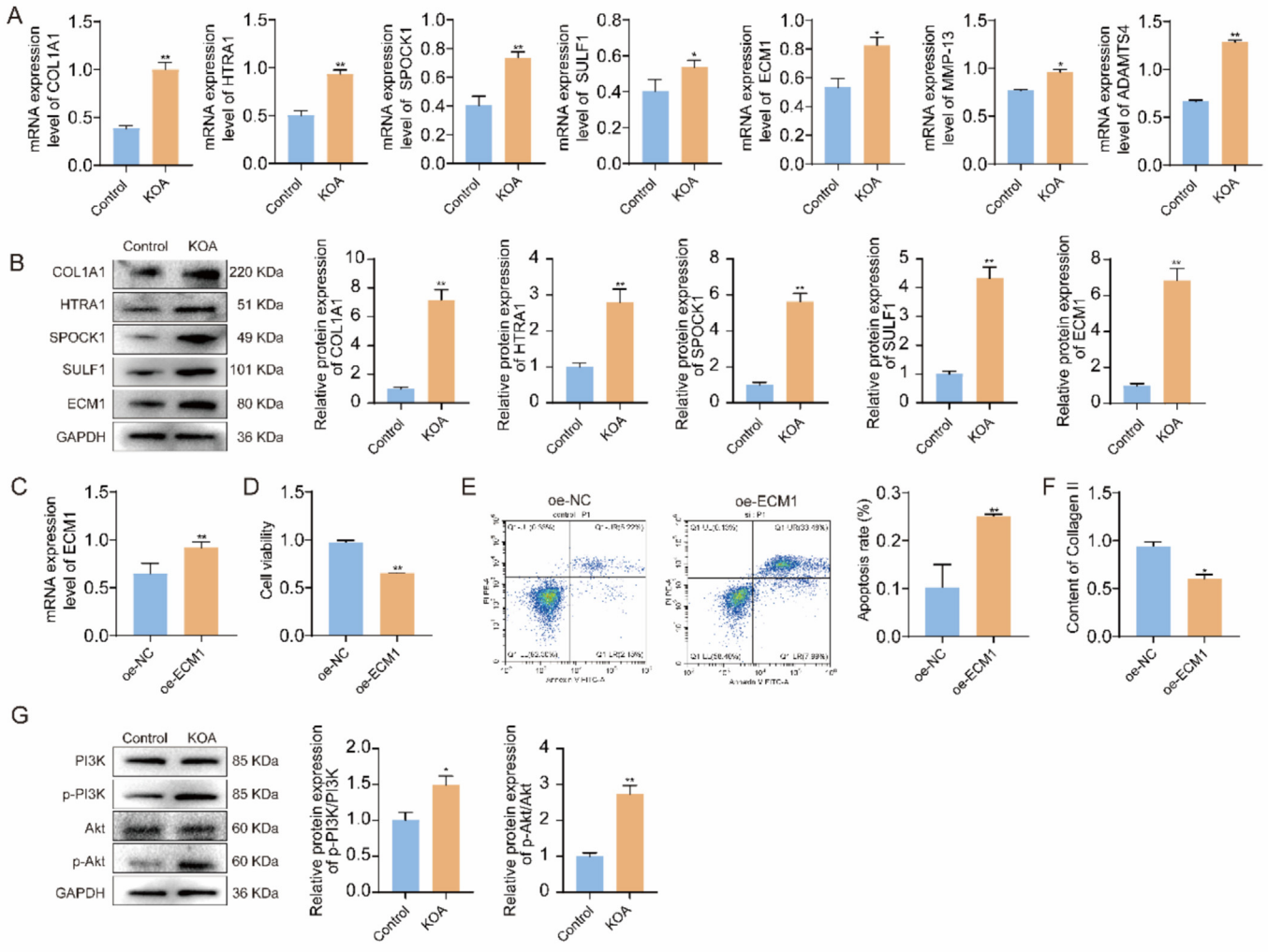

Fig. 8. ECM1 exacerbates the progression of KOA. The mRNA (A) and protein (B) levels of 5 diagnostic genes, as well as the mRNA expression levels of MMP-13 and ADAMTS4. (C) Transfection efficiency explored by qRT-PCR. (D) Viability of MIA-treated SW1353 cells measured by CCK-8. (E) Apoptosis of MIA-treated SW1353 cells measured by flow cytometry. (F) Content of Collagen II detected by ELISA. (G) Protein expression level of PI3K/Akt pathway-related markers. $^{*}p < 0.05$, $^{**}p < 0.01$. KOA: knee osteoarthritis; qRT-PCR: Quantitative reverse transcriptase polymerase chain reaction; CCK-8: Cell Counting Kit-8; ELISA: Enzyme-Linked Immunosorbent Assay; MIA: monosodium iodoacetate.

[73]. It is reported that the number of mast cells is elevated in the synovium of KOA patients [74], and mast cell activation, regulated by IgE, facilitates cartilage destruction and inflammation in OA [75]. In this study, the "ssGSEA" algorithm uncovered that the proportion of 13 immune cells presented remarkable differences between KOA and healthy samples, including macrophage, eosinophil, and mast cell. Then the relation between immune cells and immune cells or diagnostic genes and immune cells was investigated, and the results found that these 5 diagnostic genes were both strongly associated with most immune cells, containing macrophage and eosinophil. Besides, drugs that interacted with the 5 diagnostic genes were obtained through the "DSigDB" database, containing 9-Octadecenamide, Diacerein, and Rifaximin. These findings might offer a theoretical basis for the diagnosis and therapy of KOA.

Nevertheless, some limitations need to be considered. First, the function and mechanism of the other 4 diagnostic genes in KOA need to be further evaluated via *in vitro* and *in vivo* experiments, as well as the involved potential mechanism. Second, the screened immune cells and drugs should be further tested in animal or clinical trials. Third, the diagnostic value of the nomogram should be validated in other datasets.

This study screened 5 matrisome-associated diagnostic genes (COL1A1, HTRA1, SPOCK1, SULF1 and ECM1) and developed a reliable nomogram for diagnosing KOA. In addition, ECM1 could exacerbate the progression of KOA, and the PI3K-Akt signaling pathway is involved in the progression of KOA. These findings offer valuable insights into the novel diagnostic biomarkers and targeted therapies for KOA.

CRediT authorship contribution statement

Jianqiao Sun: Writing – original draft, Formal analysis, Conceptualization. **Gongchang Yu:** Formal analysis, Data curation, Conceptualization. **Yingjie Zhao:** Formal analysis, Data curation. **Jun Zhang:** Writing – review & editing, Data curation. **Bin Shi:** Writing – review & editing, Formal analysis, Conceptualization.

Ethical approval (humans)

The study protocol was approved by the Ethics Committee of the Neck-Shoulder and Lumbocrural Pain Hospital of Shandong First Medical University, with the approval number no. 20240613.

Financial support

This work was supported by the High Level Key Discipline Construction Project of the State Administration of Traditional Chinese Medicine (zyyzdxk-2013123), the Major Science and Technology Innovation Project of Shandong Province (2022CXGC020510), the Integration Development Strategy Project of Jinan City and College (JNSX2024046), and the clinical-basic joint innovation team project of Shandong First Medical University (No. CX202408).

Supplementary material

https://doi.org/10.1016/j.ejbt.2026.100710.

Data availability

Data will be made available on request.

References

[1] Giorgino R, Albano D, Fusco S, et al. Knee osteoarthritis: Epidemiology, pathogenesis, and mesenchymal stem cells: What else is new? An update. Int J Mol Sci 2023;24(7):6405. https://doi.org/10.3390/ijms24076405. PMid: 37047377.
[2] Zhu S, Qu W, He C. Evaluation and management of knee osteoarthritis. J Evid Based Med 2024;17(3):675–87. https://doi.org/10.1111/jebm.12627. PMid: 38963824.
[3] Sharma L. Osteoarthritis of the knee. N Engl J Med 2021;384(1):51–9. https://doi.org/10.1056/NEJMcp1903768. PMid: 33406330.
[4] Qiao H, Hao X, Wang G. Effects of mind-body exercise on knee osteoarthritis: A systematic review and meta-analysis of randomized controlled trials. BMC Musculoskelet Disord 2024;25(1):229. https://doi.org/10.1186/s12891-024-07278-4. PMid: 38515124.
[5] Gelber AC. Knee osteoarthritis. Ann Internal Med 2024;177(9):ITC129–44. https://doi.org/10.7326/annals-24-01249. PMid: 39250809.
[6] Li H, Kong W, Liang Y, et al. Burden of osteoarthritis in China, 1990–2019: Findings from the Global Burden of Disease Study 2019. Clin Rheumatol 2024;43(3):1189–97. https://doi.org/10.1007/s10067-024-06885-9. PMid: 38289570.
[7] Jang S, Lee K, Ju JH. Recent updates of diagnosis, pathophysiology, and treatment on osteoarthritis of the knee. Int J Mol Sci 2021;22(5):2619. https://doi.org/10.3390/ijms22052619. PMid: 33807695.
[8] Tore NG, Oskay D, Haznedaroglu S. The quality of physiotherapy and rehabilitation program and the effect of telerehabilitation on patients with knee osteoarthritis. Clin Rheumatol 2023;42(3):903–15. https://doi.org/10.1007/s10067-022-06417-3. PMid: 36279075.
[9] Deng M, Hu Y, Zhang Z, et al. Unicondylar knee replacement versus total knee replacement for the treatment of medial knee osteoarthritis: A systematic review and meta-analysis. Arch Orthop Trauma Surg 2021;141(8):1361–72. https://doi.org/10.1007/s00402-021-03790-7. PMid: 33512583.
[10] Theocharis AD, Skandalis SS, Gialeli C, et al. Extracellular matrix structure. Adv Drug Deliv Rev 2016;97:4–27. https://doi.org/10.1016/j.addr.2015.11.001. PMid: 26562801.
[11] Famá EAB, Pinhal MAS. Extracellular matrix components in preeclampsia. Clin Chim Acta 2025;568:120132. https://doi.org/10.1016/j.cca.2025.120132. PMid: 39798685.
[12] Li SH, Wu QF. MicroRNAs target on cartilage extracellular matrix degradation of knee osteoarthritis. Eur Rev Med Pharmacol Sci 2021;25(3):1185–97. https://doi.org/10.26355/eurrev_202102_24821. PMid: 33629288.
[13] Arteel GE, Naba A. The liver matrisome – looking beyond collagens. JHEP Rep 2020;2(4):100115. https://doi.org/10.1016/j.jhepr.2020.100115. PMid: 32637906.
[14] Downs M, Sethi MK, Raghunathan R, et al. Matrisome changes in Parkinson's disease. Anal Bioanal Chem 2022;414(9):3005–15. https://doi.org/10.1007/s00216-022-03929-4. PMid: 35112150.
[15] Wise CA, Sepich D, Ushiki A, et al. The cartilage matrisome in adolescent idiopathic scoliosis. Bone Res 2020;8:13. https://doi.org/10.1038/s41413-020-0089-0. PMid: 32195011.
[16] Rafaeva M, Erler JT. Framing cancer progression: Influence of the organ- and tumour-specific matrisome. FEBS J 2020;287(8):1454–77. https://doi.org/10.1111/febs.15223. PMid: 31972068.
[17] Sung JY, Cheong JH. The matrisome is associated with metabolic reprograming in stem-like phenotypes of gastric cancer. Cancers 2022;14(6):1438. https://doi.org/10.3390/cancers14061438. PMid: 35326589.
[18] Miosge N, Hartmann M, Maelicke C, et al. Expression of collagen type I and type II in consecutive stages of human osteoarthritis. Histochem Cell Biol 2004;122(3):229–36. https://doi.org/10.1007/s00418-004-0697-6. PMid: 15316793.
[19] Xia B, Di C, Zhang J, et al. Osteoarthritis pathogenesis: A review of molecular mechanisms. Calcif Tissue Int 2014;95(6):495–505. https://doi.org/10.1007/s00223-014-9917-9. PMid: 25311420.
[20] Meszaros E, Malemud CJ. Prospects for treating osteoarthritis: Enzyme-protein interactions regulating matrix metalloproteinase activity. Ther Adv Chronic Dis 2012;3(5):219–29. https://doi.org/10.1177/2040622312454157. PMid: 23342237.
[21] Chen W, Liu W, Jiang T, et al. Tongbi Huoluo Decoction alleviates cartilage degeneration in knee osteoarthritis by inhibiting degradation of extracellular matrix. Chin Med 2023;18(1):91. https://doi.org/10.1186/s13020-023-00802-z. PMid: 37507774.
[22] Han W, Chen X, Wang X, et al. TLR-4, TLR-5 and IRF4 are diagnostic markers of knee osteoarthritis in the middle-aged and elderly patients and related to disease activity and inflammatory factors. Exp Ther Med 2020;20(2):1291–8. https://doi.org/10.3892/etm.2020.8825. PMid: 32765669.
[23] Hassan MA, Hameed AS, Hameed EK. Serum fibulin-3 as a diagnostic and prognostic biomarker in patients with knee osteoarthritis. Ir J Med Sci 2024;193(6):2923–7. https://doi.org/10.1007/s11845-024-03780-9. PMid: 39127857.
[24] Leek JT, Johnson WE, Parker HS, et al. The sva package for removing batch effects and other unwanted variation in high-throughput experiments. Bioinformatics 2012;28(6):882–3. https://doi.org/10.1093/bioinformatics/bts034. PMid: 22257669.
[25] Ritchie ME, Phipson B, Wu D, et al. *limma* powers differential expression analyses for RNA-sequencing and microarray studies. Nucl Acids Res 2015;43(7):e47. https://doi.org/10.1093/nar/gkv007. PMid: 25605792.
[26] Hu Y, Shao X, Xing L, et al. Single-cell sequencing of lung macrophages and monocytes reveals novel therapeutic targets in COPD. Cells 2023;12(24):2771. https://doi.org/10.3390/cells12242771. PMid: 38132091.
[27] Li Z, Song G, Guo D, et al. Identification of GINS2 prognostic potential and involvement in immune cell infiltration in hepatocellular carcinoma. J Cancer 2022;13(2):610–22. https://doi.org/10.7150/jca.53841. PMid: 35069907.
[28] Langfelder P, Horvath S. WGCNA: An R package for weighted correlation network analysis. BMC Bioinf 2008;9:559. https://doi.org/10.1186/1471-2105-9-559. PMid: 19114008.
[29] Tian Z, He W, Tang J, et al. Identification of important modules and biomarkers in breast cancer based on WGCNA. OncoTargets Therapy 2020;13:6805–17. https://doi.org/10.2147/ott.S258439. PMid: 32764968.
[30] Chang YT, Hong ZJ, Tsai HH, et al. Hub metastatic gene signature and risk score of breast cancer patients with small tumor sizes using WGCNA. Breast Cancer 2024;31(6):1114–29. https://doi.org/10.1007/s12282-024-01627-w. PMid: 39190284.
[31] Naba A, Clauser KR, Hoersch S, et al. The matrisome: *In silico* definition and *in vivo* characterization by proteomics of normal and tumor extracellular matrices. Mol Cell Proteom 2012;11(4):M111.014647. https://doi.org/10.1074/mcp.M111.014647. PMid: 22159717.
[32] Yu G, Wang LG, Han Y, et al. clusterProfiler: An R package for comparing biological themes among gene clusters. OMICS J Integr Biol 2012;16(5):284–7. https://doi.org/10.1089/omi.2011.0118. PMid: 22455463.
[33] Mering C, Huynen M, Jaeggi D, et al. STRING: A database of predicted functional associations between proteins. Nucl Acids Res 2003;31(1):258–61. https://doi.org/10.1093/nar/gkg034. PMid: 12519996.
[34] Su Y, Zhang Y. Identification of biological processes and genes for gestational diabetes mellitus. Arch Gynecol Obstet 2015;292(3):635–40. https://doi.org/10.1007/s00404-015-3649-6. PMid: 25736406.
[35] Shannon P, Markiel A, Ozier O, et al. Cytoscape: A software environment for integrated models of biomolecular interaction networks. Genome Res 2003;13(11):2498–504. https://doi.org/10.1101/gr.1239303. PMid: 14597658.
[36] Kang J, Choi YJ, Kim IK, et al. LASSO-based machine learning algorithm for prediction of lymph node metastasis in T1 colorectal cancer. Cancer Res Treat 2021;53(3):773–83. https://doi.org/10.4143/crt.2020.974. PMid: 33421980.
[37] Naveed S. Prediction of breast cancer through random forest. Curr Med Imaging 2023;19(10):1144–55. https://doi.org/10.2174/1573405618666220930150625. PMid: 36200251.
[38] Sanz H, Valim C, Vegas E, et al. SVM-RFE: Selection and visualization of the most relevant features through non-linear kernels. BMC Bioinf 2018;19(1):432. https://doi.org/10.1186/s12859-018-2451-4. PMid: 30453885.
[39] Jiang B, Sun P, Tang J, et al. GLMNet: Graph learning-matching networks for feature matching. Pattern Recogn 2022;121:108167. https://doi.org/10.1016/j.patcog.2021.108167.
[40] Liaw A, Wiener M. Classification and regression by randomForest. The R Journal 2002;2–3:18–22.
[41] Functions TM, Wien TU. Package 'e1071'; 2012.
[42] Robin X, Turck N, Hainard A, et al. pROC: An open-source package for R and S+ to analyze and compare ROC curves. BMC Bioinf 2011;12:77. https://doi.org/10.1186/1471-2105-12-77. PMid: 21414208.
[43] Kattan MW, Marasco J. What is a real nomogram? Semin Oncol 2010;37(1):23–6. https://doi.org/10.1053/j.seminoncol.2009.12.003. PMid: 20172360.
[44] Tibshirani R. The LASSO method for variable selection in the Cox Model. Stat Med 1997;16(4):385–95. https://doi.org/10.1002/(SICI)1097-0258(19970228)16:4<385::AID-SIM380>3.0.CO;2-3. PMid: 9044528.
[45] Zheng Y, Wang J, Ling Z, et al. A diagnostic model for sepsis-induced acute lung injury using a consensus machine learning approach and its therapeutic implications. J Transl Med 2023;21(1):620. https://doi.org/10.1186/s12967-023-04499-4. PMid: 37700323.

[46] Yoo M, Shin J, Kim J, et al. DSigDB: Drug signatures database for gene set analysis. Bioinformatics 2015;31(18):3069–71. https://doi.org/10.1093/bioinformatics/btv313. PMid: 25990557.
[47] Xiao B, Liu L, Li A, et al. Identification and verification of immune-related gene prognostic signature based on ssGSEA for osteosarcoma. Front Oncol 2020;10:607622. https://doi.org/10.3389/fonc.2020.607622. PMid: 33384961.
[48] Qiu C, Shi W, Wu H, et al. Identification of molecular subtypes and a prognostic signature based on inflammation-related genes in colon adenocarcinoma. Front Immunol 2021;12:769685. https://doi.org/10.3389/fimmu.2021.769685. PMid: 350030.
[49] Rockel JS, Sharma D, Espin-Garcia O, et al. Deep learning-based clustering for endotyping and post-arthroplasty response classification using knee osteoarthritis multiomic data. Ann Rheum Dis 2025;84(5):844–55. https://doi.org/10.1016/j.ard.2025.01.012. PMid: 39948003.
[50] Farrar JT, Young JP, LaMoreaux L, et al. Clinical importance of changes in chronic pain intensity measured on an 11-point numerical pain rating scale. Pain 2001;94(2):149–58. https://doi.org/10.1016/s0304-3959(01)00349-9. PMid: 11690728.
[51] Chiu PR, Hu YC, Huang TC, et al. Vitamin C protects chondrocytes against monosodium iodoacetate-induced osteoarthritis by multiple pathways. Int J Mol Sci 2016;18(1):38. https://doi.org/10.3390/ijms18010038. PMid: 28035982.
[52] Wang L, Li S, Luo H, et al. PCSK9 promotes the progression and metastasis of colon cancer cells through regulation of EMT and PI3K/AKT signaling in tumor cells and phenotypic polarization of macrophages. J Exp Clin Cancer Res 2022;41(1):303. https://doi.org/10.1186/s13046-022-02477-0. PMid: 36242053.
[53] Darzynkiewicz Z, Bedner E, Smolewski P. Flow cytometry in analysis of cell cycle and apoptosis. Semin Hematol 2001;38(2):179–93. https://doi.org/10.1016/s0037-1963(01)90051-4. PMid: 11309699.
[54] Hornbeck PV. Enzyme-linked immunosorbent assays. Curr Protocols Immunol 2015;110:2.1–2.1.23. https://doi.org/10.1002/0471142735.im0201s110. PMid: 26237010.
[55] Ma H, Bell KN, Loker RN. qPCR and qRT-PCR analysis: Regulatory points to consider when conducting biodistribution and vector shedding studies. Mol Ther Methods Clin Dev 2021;20:152–68. https://doi.org/10.1016/j.omtm.2020.11.007. PMid: 33473355.
[56] Mahmoudian A, King LK, Liew JW, et al. Timing is everything: Towards classification criteria for early-stage symptomatic knee osteoarthritis. Osteoarthr Cartil 2024;32(6):649–53. https://doi.org/10.1016/j.joca.2024.02.888. PMid: 38437945.
[57] Nersisyan S, Novosad V, Engibaryan N, et al. ECM-receptor regulatory network and its prognostic role in colorectal cancer. Front Genet 2021;12:782699. https://doi.org/10.3389/fgene.2021.782699. PMid: 34938324.
[58] Chen C, Chen J, Wang Y, et al. *Ganoderma lucidum* polysaccharide inhibits HSC activation and liver fibrosis via targeting inflammation, apoptosis, cell cycle, and ECM-receptor interaction mediated by TGF-β/Smad signaling. Phytomedicine 2023;110:154626. https://doi.org/10.1016/j.phymed.2022.154626. PMid: 36603342.
[59] Zhong J, Xiang D, Ma X. Prediction and analysis of osteoarthritis hub genes with bioinformatics. Ann Transl Med 2023;11(2):66. https://doi.org/10.21037/atm-22-6450. PMid: 36819525.
[60] Li J, Jiang M, Yu Z, et al. Artemisinin relieves osteoarthritis by activating mitochondrial autophagy through reducing *TNFSF11* expression and inhibiting PI3K/AKT/mTOR signaling in cartilage. Cell Mol Biol Lett 2022;27(1):62. https://doi.org/10.1186/s11658-022-00365-1. PMid: 3590282.
[61] Xu K, He Y, Moqbel SAA, et al. SIRT3 ameliorates osteoarthritis via regulating chondrocyte autophagy and apoptosis through the PI3K/Akt/mTOR pathway. Int J Biol Macromol 2021;175:351–60. https://doi.org/10.1016/j.ijbiomac.2021.02.029. PMid: 33556400.
[62] Chen Y, Pan X, Zhao J, et al. Icariin alleviates osteoarthritis through PI3K/Akt/mTOR/ULK1 signaling pathway. Eur J Med Res 2022;27(1):204. https://doi.org/10.1186/s40001-022-00820-x. PMid: 36253872.
[63] Wang K, Li Y, Lin J. Identification of diagnostic biomarkers for osteoarthritis through bioinformatics and machine learning. Heliyon 2024;10(6):e27506. https://doi.org/10.1016/j.heliyon.2024.e27506. PMid: 38496843.
[64] Li X, Sun X, Kan C, et al. COL1A1: A novel oncogenic gene and therapeutic target in malignancies. Pathol Res Pract 2022;236:154013. https://doi.org/10.1016/j.prp.2022.154013. PMid: 35816922.
[65] Aborehab NM, El Bishbishy MH. Chondroprotection of fruit peels in a monosodium iodoacetate-induced osteoarthritis rat model via downregulation of Col1A1. Arch Pharm 2022;355(7):e2200028. https://doi.org/10.1002/ardp.202200028. PMid: 35385163.
[66] Oka C, Saleh R, Bessho Y, et al. Interplay between HTRA1 and classical signalling pathways in organogenesis and diseases. Saudi J Biol Sci 2022;29(4):1919–27. https://doi.org/10.1016/j.sjbs.2021.11.056. PMid: 35531175.
[67] Murayama M, Hirata H, Shiraki M, et al. Nupr1 deficiency downregulates HtrA1, enhances SMAD1 signaling, and suppresses age-related bone loss in male mice. J Cell Physiol 2023;238(3):566–81. https://doi.org/10.1002/jcp.30949. PMid: 36715607.
[68] Otsuki S, Taniguchi N, Grogan SP, et al. Expression of novel extracellular sulfatases Sulf-1 and Sulf-2 in normal and osteoarthritic articular cartilage. Arthritis Res Ther 2008;10(3):R61. https://doi.org/10.1186/ar2432. PMid:18507859.
[69] Feng D, Li H, Ma X, et al. Downregulation of extracellular matrix protein 1 effectively ameliorates osteoarthritis progression *in vivo*. Int Immunopharmacol 2024;126:111291. https://doi.org/10.1016/j.intimp.2023.111291. PMid: 38039715.
[70] Xie J, Huang Z, Yu X, et al. Clinical implications of macrophage dysfunction in the development of osteoarthritis of the knee. Cytokine Growth Factor Rev 2019;46:36–44. https://doi.org/10.1016/j.cytogfr.2019.03.004. PMid: 30910350.
[71] Zhang H, Lin C, Zeng C, et al. Synovial macrophage M1 polarisation exacerbates experimental osteoarthritis partially through R-spondin-2. Ann Rheum Dis 2018;77(10):1524–34. https://doi.org/10.1136/annrheumdis-2018-213450. PMid: 29991473.
[72] Blackler G, Lai-Zhao Y, Klapak J, et al. Targeting STAT6-mediated synovial macrophage activation improves pain in experimental knee osteoarthritis. Arthritis Res Ther 2024;26(1):73. https://doi.org/10.1186/s13075-024-03309-6. PMid: 38509602.
[73] Ravin KA, Loy M. The eosinophil in infection. Clin Rev Allergy Immunol 2016;50(2):214–27. https://doi.org/10.1007/s12016-015-8525-4. PMid: 26690368.
[74] Uchida K, Takano S, Inoue G, et al. Increase in mast cell marker expression in the synovium of obese patients with osteoarthritis of the knee. Diabetes Metab Syndr Obesity Targets Therapy 2019;12:377–82. https://doi.org/10.2147/dmso.S201523. PMid: 31114272.
[75] Wang Q, Lepus CM, Raghu H, et al. IgE-mediated mast cell activation promotes inflammation and cartilage destruction in osteoarthritis. eLife 2019;8:e39905. https://doi.org/10.7554/eLife.39905. PMid: 31084709.